Chapter 2

As described in the first chapter, the ionization of neutral targets by fast charged projectiles is a process for which there exists an extensive body of work, both experimental and theoretical. Within the rich history of electron spectroscopy, very few measurements exist for energies below 10 eV. The purpose of this chapter is to report our early measurements of all three components of the momentum vector of soft electrons produced in ionizing collisions. These experiments began in the summer of 1996, and were published in the proceedings of the 1996 conference *Application of Accelerators in Research and Industry* [2.1].

Measurements with conventional spectrometers have been limited to the method used to study ejected electrons of low energy due to the dispersive nature of the differential cross section $d^2\sigma/dEd\Omega$. The idea behind our experiments is to project the low energy electrons with an external electric field onto a detector. We measure the distribution of electron flight times, thereby taking advantage of the nondispersive cross section $d\sigma/dt \Rightarrow d\sigma/dp_x$ (throughout we use the convention that the electric field is in the x-direction). In addition to the electron's flight time, we can measure its final position on the detector, which leads the other components of the

momentum vector ($d\sigma/dz \Rightarrow d\sigma/dp_z$, $d\sigma/dy \Rightarrow d\sigma/dp_y$). We will explain the details of these relationships later in the chapter.

The difficulty with this method, however, is that electrons have very little mass. In order to collect them on the detector, a substantial electric field must be applied. This gives the electrons a large acceleration, which in turn makes the flight times very short. The technological advance that made this research possible was the use of a super-conducting linear accelerator (LINAC) to "superbunch" the projectile ion beam, allowing us to measure the electron flight time. This technique is described in appendix C.

Conventional electron spectroscopy techniques provide limited or no information about the other participants in the collision. For example, because the final charge state of the target atom is not observed, distinction between single and multiple ionization is not possible. For these initial experiments, our technique allowed us to measure the recoil ion flight time. In our spectrometer, recoil ions of differing charge to mass ratios have different accelerations causing their associated flight times to be different. Thus, we were able to separate the final target charge states. This illustration gives only a glimpse of the power of this technique. In later chapters we describe how a local target is introduced. In that case, the full recoil-ion momentum vector may be measured as well, and the advantage of using momentum imaging to measure electrons will become apparent.

For the present experiment, the collision systems that we studied were chosen primarily because a group in our laboratory had results readily available with which

we could compare. Using a multi-stage electron spectrometer, Tribedi *et al* measured electron spectra at various angles for bare 2.5 MeV/u carbon projectiles colliding with helium and hydrogen targets [1.1, 2.2-2.4]. By converting the angle and energy distributions to momentum distributions and vice versa, comparison of the results from each experiment was straightforward. We must emphasize at this point, that the Tribedi results are integrated to the upper energy limits of their measurements (> 1 keV), whereas our results were restricted to less than 30 eV. However, as can be seen from figure 1.3, this corresponds to more than 85% of the cross section and will adequately serve our purpose.

2.1 Apparatus and Method

A bunched beam of C^{6+} projectiles was accelerated to 30 MeV by the J.R. Macdonald EN Tandem Van de Graaff Accelerator. In order to measure the electron flight time relative to the projectile, the beam was bunched and time focused by the KSU LINAC (Appendix C). For the present work, the width of the bunches was measured to be less than 0.4 nsec. This beam was then tightly collimated, and directed into a target region of diffuse gas. Ejected electrons and recoil ions produced in the target region were extracted and accelerated in opposite directions toward position sensitive microchannel plate detectors by a uniform electric field (between 30 and 425 V/cm). Both detectors were oriented perpendicular to the beam (Fig. 2.1).

spectrometer

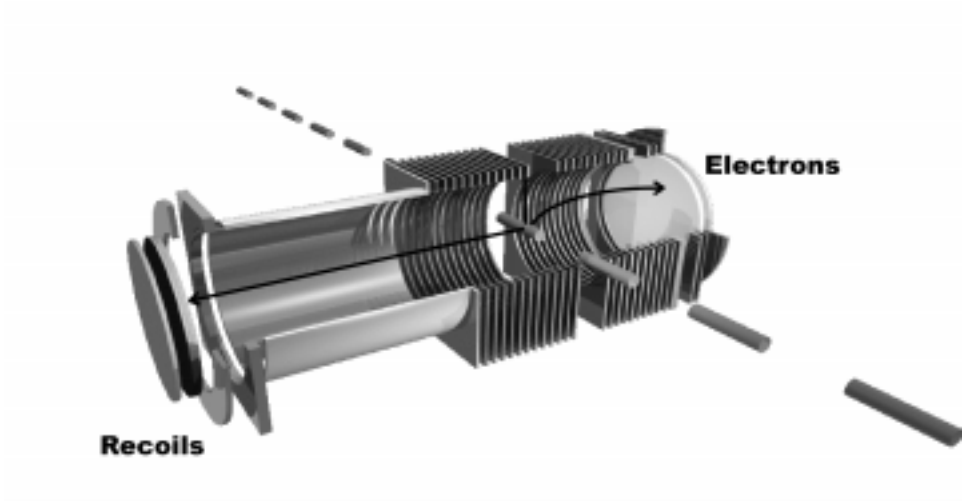

Figure 2.1: Scale drawing of electron momentum imaging spectrometer. Bunch duty cycle is not to scale for the purpose of visualization.

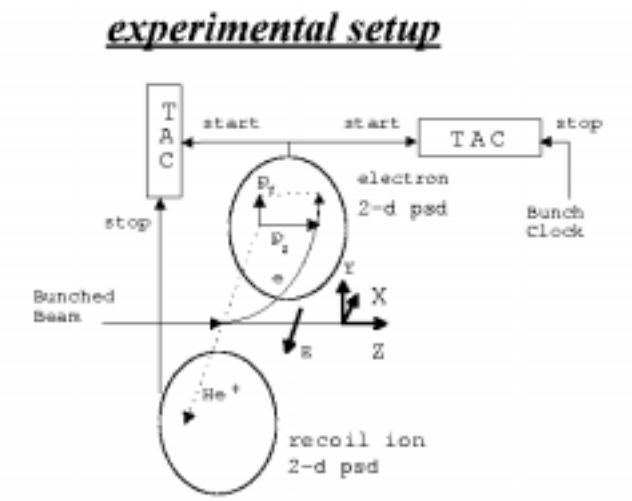

Figure 2.2: Experimental Arrangement for electron momentum imaging. The collision point was determined by the position on the recoil detector assuming a straight-line recoil trajectory. Note the coordinate system.

As can be seen in figure 2.2, we have chosen a convenient coordinate system such that the z-axis is defined by the beam, the x-axis is defined by the direction of the electric field, and the y-axis is perpendicular to both. This results in the detectors lying parallel to the y-z plane. Therefore, the actual quantities we measured were the y- and z- position of both the electron and recoil ion, as well as their times-of-flight (TOF_e, TOF_R). TOF_e was measured relative to a start signal synchronized with the beam bunch, while the much longer TOF_R was measured relative to the electron time signal.

In order to determine the electron momentum, we required the electron position relative to the collision. It was determined in the following way. The low energy (~1 meV) target recoils were accelerated in the electric field of the spectrometer. Due to their large mass and the high electric field, they traveled in nearly straight-line trajectories to the recoil detector. This pinpointed the origin of the ionization event. The recoil z-position (birthplace of the electron along the beam axis) was then subtracted from the electron z-position to yield the true electron position relative to the collision point. Due to the symmetry of the spectrometer, the corresponding y-position of the electron is simply measured from the center of its distribution. This is done because the width of the collimated beam is less than the resolution of the recoil detector.

The resulting (y, z) position in conjunction with the electron time of flight is used to determine the (y, z) momentum by the following equations:

$$P_y = \frac{my}{t} \qquad P_z = \frac{mz}{t} \tag{2.1}$$

where m and t are the electron mass and TOF_e respectively. The electrons are accelerated through a uniform electric field from the collision point to the detector. Therefore, the momentum component along the electric field vector (x-axis) is determined solely from TOF_e, the spectrometer dimensions and the magnitude of the electric field. These are related by the equation:

$$P_x = \frac{md}{t} - \frac{eEt}{2} \tag{2.2}$$

where E is the electric field, t is TOF_e, and d is the distance from the collision point to the electron detector. The quantities m and e are the electron mass and charge respectively.

The resolution of the electron momentum depends on several factors. Along the x-axis, assuming small momenta, the resolution is governed by the impulse equation:

$$\Delta P_x = -eE\,\Delta t \tag{2.3}$$

with the same notation used previously. For example, a time resolution of 1 nsec and a field of 100 V/cm yields a momentum resolution along the field axis of approximately 0.8 atomic units (a.u.). The resolution of the y- and z-momenta is dominated by the position resolution of the detectors:

$$\Delta P_y = \frac{m\,\Delta y}{t_0} \qquad \Delta P_Z = \frac{m\,\Delta y}{t_0} \tag{2.4}$$

where the notation is the same as above with t_0 representing the TOF for $P_x = 0$. The typical resolution for the wedge and strip type anodes that we used is 0.5 mm. Taking this value and a typical electron flight time of 10 nsec, the resulting momentum resolution is 0.2 a.u.

2.2 Results and Conclusions

Shown in figure 2.3 are the flight time spectra for both collision systems. For a given electric field, the following equation governing the recoil flight time holds:

$$t_R \propto \sqrt{\frac{m_R}{q_R}} \tag{2.5}$$

where t_R, m_R, and q_R are the recoil ion flight time, mass and charge respectively.

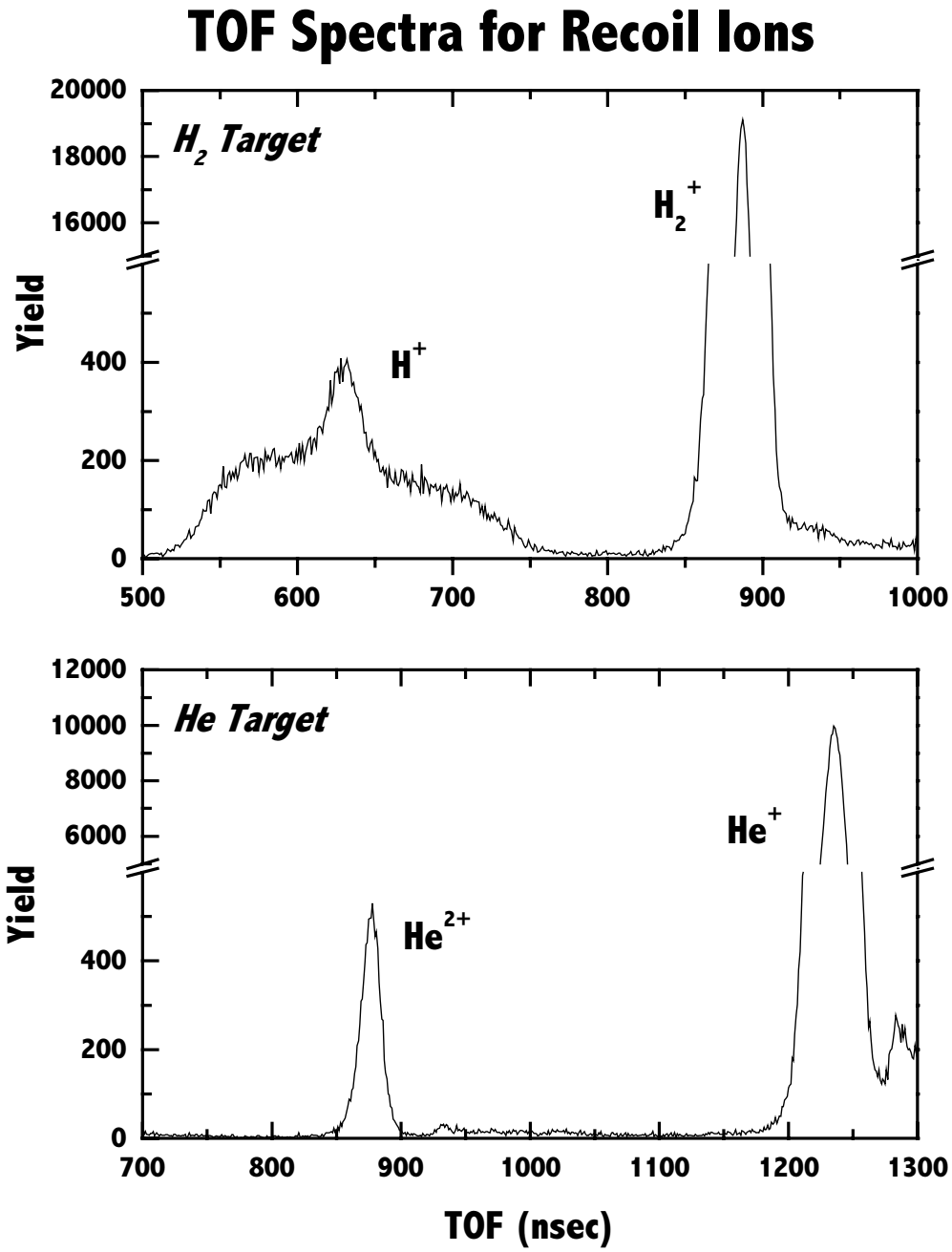

Figure 2.3: Recoil ion time of flight spectra. Note the clear charge state separation. The broadness of the H^+ peak is due to the molecular fragment coulomb explosion.

Figure 2.3 shows two typical recoil ion time-of-flight spectra. One can see a clear separation of the recoil states in the spectra. The large difference in the relative size of the peaks confirms that double ionization is a small part of the cross section for both collision systems. In the hydrogen spectrum, one prominent feature is the broadness of the H^+ peak. This is due to molecular effects that will be discussed in more detail in Chapter 3.

In general, the width of each peak is representative of the recoil ion momentum distribution along the field axis, coupled with the width of the beam and the resolution of the time measurement. For the purpose of this experiment however, we were primarily concerned with the separation of the recoil charge states. We will discuss the use of the time information to its full extent in chapters 3 and 4. Because the data was taken in event mode (see appendix F), we were able to set a gate on a particular recoil charge state in the offline analysis and study the corresponding electron spectra. However, as we were motivated at this point to prove the principle of operation, we did not focus on any particular physical phenomenon (e.g. double ionization of helium).

Figure 2.4 shows a typical raw position spectrum from the recoil ion detector. Because the beam interacted with target gas along its entire path through the spectrometer, a horizontal line of recoils along that path can be seen on the detector. We used this position signal to determine the original position of the collision event.

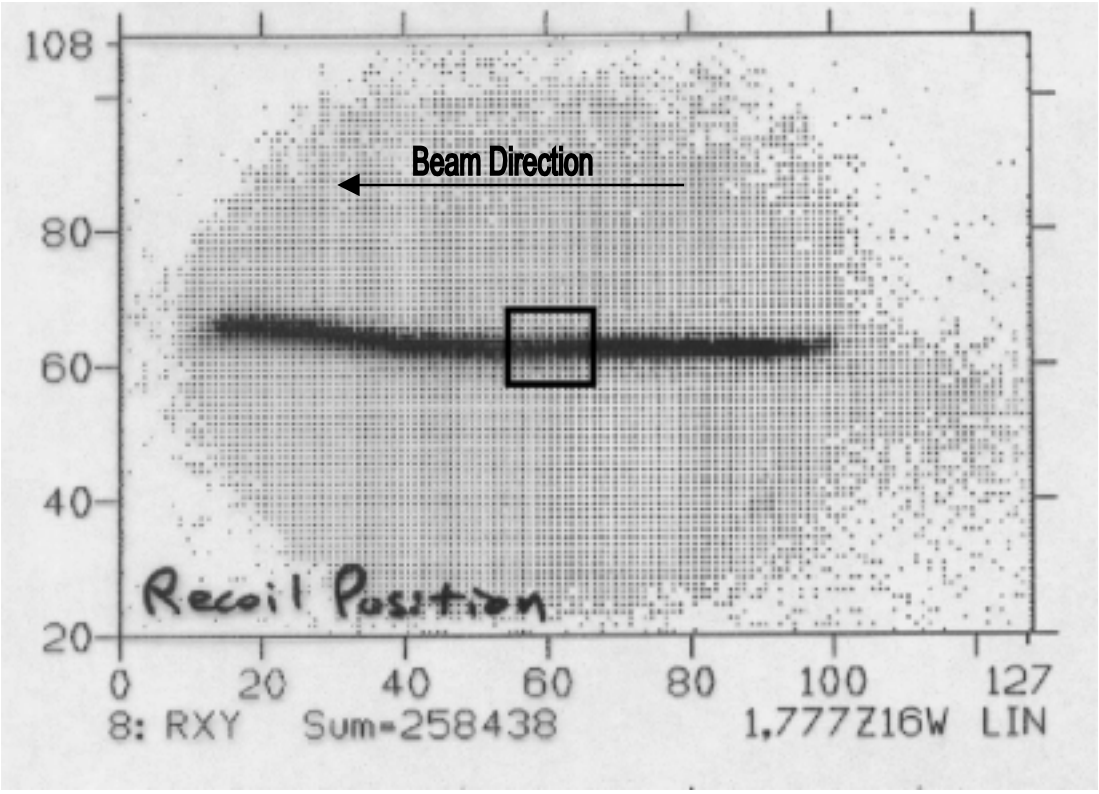

Figure 2.4: Typical spectrum of the raw recoil detector image. The horizontal line is produced from recoil ions along the path of the beam through the diffuse gas. A sample recoil gate is also shown.

In order to insure that the electrons came from the central region of the spectrometer, a gate was placed on the central portion of the recoil position such as shown in the figure. The recoil detector does show some distortion, particularly apparent at the left-hand or downstream side of the detector. However, for the purposes of this measurement, the quality of the position measurement was adequate. For later experiments, when information on the recoil ion position became more critical, this problem was diagnosed and corrected.

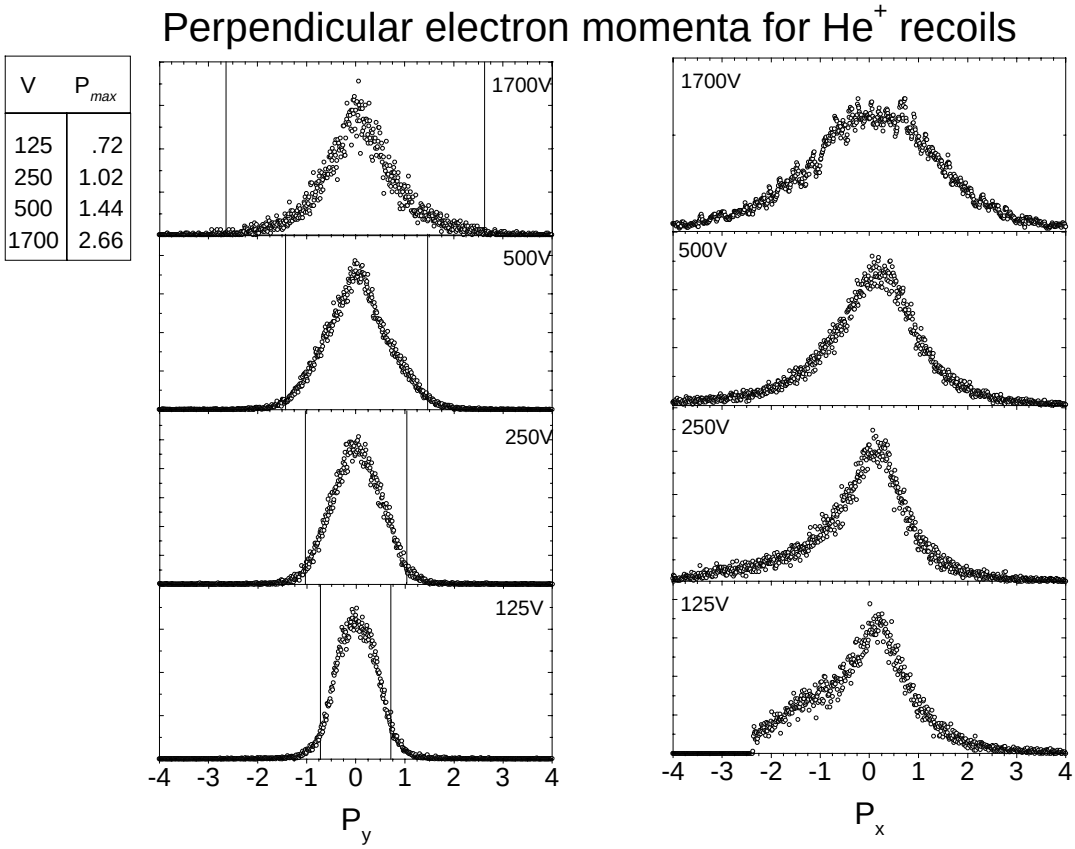

Figure 2.5: Perpendicular electron momentum spectra for various pusher voltages. In the case of high voltage, the resolution in x becomes poor, and for low voltage, the detector size in momentum space becomes small.

The primary goal of these measurements was to determine if we could produce fully three-dimensional electron spectra through the use of momentum imaging. A good test of this was to compare momentum spectra for the two components perpendicular to the beam. The collision system along the beam axis is cylindrically symmetric. Therefore, the momentum distributions in x and y should be identical. Shown in figure 2.5 are these distributions for a variety of accelerating fields. From equation 2.3, we know that as the electric field becomes large, the momentum resolution in the x-direction increases. This is apparent in the broadening of the P_x distribution as the pusher voltage increases.

We can estimate the total experimental time resolution in the following way. We assume the momentum distribution along the field (P_x) at 250V to have the true width. We approximate the conversion from time to momentum as linear (this is not exact, but sufficient for this estimate). Because the broadening of the 1700V case is due to time resolution, we have the following using equation 2.3:

$$\left(\Delta P_{res}\right)^2 = \left(eE\,\Delta t\right)^2 = \left(\Delta P_{1700V}\right)^2 - \left(\Delta P_{250V}\right)^2 \qquad (2.6)$$

Taking E=1700V/4cm, the resultant time resolution for this case is Δt=0.84 nsec. The time width of the projectile ion bunches was less than 0.4 nsec, which is within the accuracy of this estimate. Additional width in the time resolution is attributed to the electronics.

Another effect caused by changing the electric field is the change in size of the detector in momentum space. Equation 2.1 shows that as TOF_e changes with

changing electric field, the conversion from position to momentum is affected. The vertical bars shown with the P_y distributions represent where the edge of the detector would lie in momentum space The electron detector was round, and had an active area with diameter 38 mm. We simulated the detector to be a 38 mm square. The resultant edge in momentum space was calculated using TOF_e for an electron with zero momentum. The values are shown in the table in figure 2.5.

From these results, we see that a balance must be struck between the assurance that all of the electrons get on the detector and a low enough field that the P_x measurement is acceptable. The field at 1700V case is clearly too large, and the field at 250V is too small. For this reason, we took the majority of our data at 500V. One remedy for this situation is to place the electron detector closer to the collision region. We incorporated this change into the apparatus used for the experiments described in chapter 4.

Shown in figure 2.6 are the longitudinal momentum spectra from our measurements, and those determined from the conventional spectroscopic measurements made by Tribedi *et al*. For the purpose of these comparisons, we normalized our data to those of Tribedi. In addition, the zero-position of the electron detector relative to the recoil detector is not well known. To correct for this, we shifted our spectra to match the Tribedi results. Although we normalized and shifted our data the width and shape of the distribution were left as measured. Our helium results appear to be broader than those of Tribedi, while the hydrogen data matches extremely well.

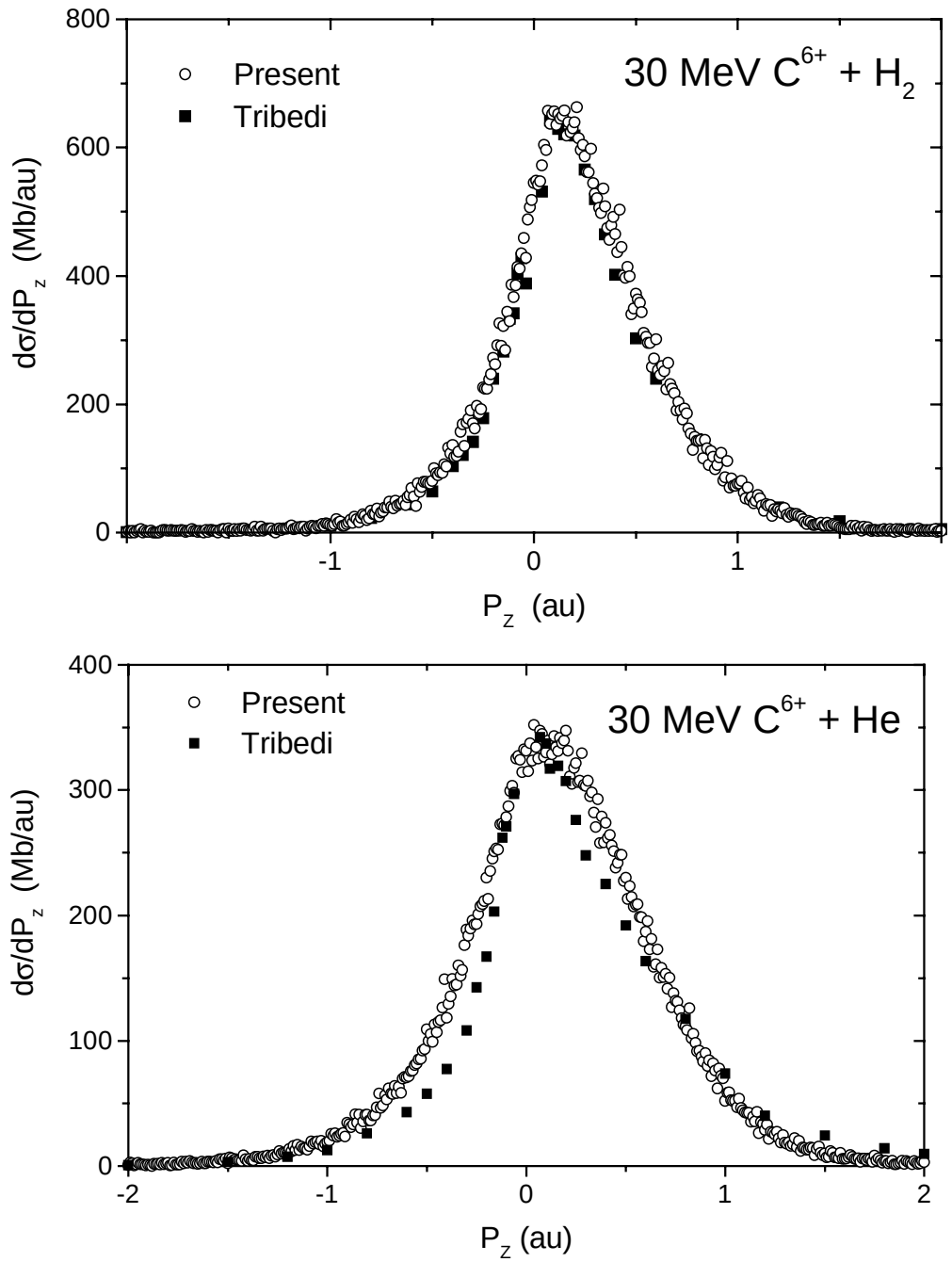

Figure 2.6: Comparisons of cross sections differential in longitudinal momentum between our present result and Tribedi *et al*. Our results were normalized to match the peak height in the Tribedi data, and shifted to match the P_z=0.

Figure 2.7 is a comparison between our results and those of Tribedi (again, integrated to large E_e) for the angular distributions of the electrons. For our data set, the angle was determined by taking the arctangent of the quotient of the transverse and longitudinal momenta. Because of this conversion, these spectra are a more sensitive test of the agreement of the two data sets. In both cases, our results were scaled to roughly follow those of Tribedi. In the helium spectrum the agreement is far from perfect, but one can see that the data follow the same general shape. This deviation is at least in part due to the broadening in the longitudinal momentum measurement. The hydrogen results, however, are in much better agreement as in the momentum spectrum. In any event, there is sufficient evidence to conclude that we were successful in our use of a momentum imaging technique to measure these electron spectra.

In conclusion, we have shown an imaging technique can be used to measure full three-dimensional momentum vectors of soft electrons spectra is possible. We had the good fortune to be in the same laboratory as a group doing state-of-the-art conventional electron measurements. A comparison of our data with that of Tribedi gave ample evidence that our experiment was successful. It is important to emphasize that measurements in the low energy regime by Tribedi are state-of-the-art and not typical of conventional spectroscopy. For further reading, we refer you to the letter by Schmitt et al [2.5], in which they report detailed measurements of the “target cusp” using a similar momentum imaging method.

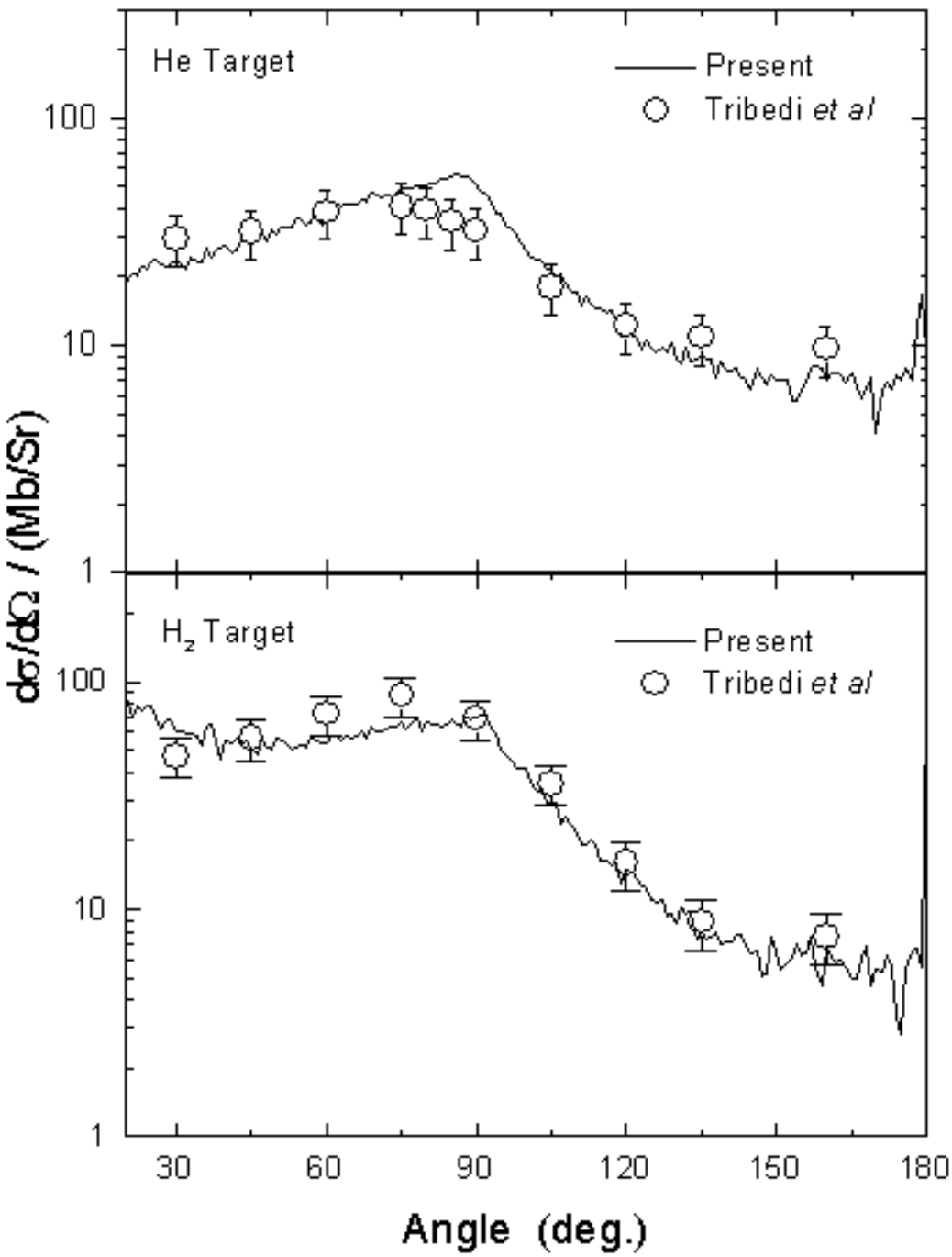

Figure 2.7: Comparisons of cross sections differential in angle between our present result and Tribedi *et al*. Our results are scaled to those of Tribedi.

The next chapters will describe in detail experiments that were in essence the offspring of this early work and unleashed the full capabilities of this technique. The most significant improvement made to the apparatus was the addition of a gas jet. This local (and cold) target enabled the momentum measurement of the *recoil-ion*. In the case of a diatomic molecular target, the recoil momentum vector implies the spatial alignment of the internuclear axis relative to the beam axis. In the case of a helium target, the simultaneous measurement of both the recoil momentum vector and the electron momentum vector infers the momentum transfer to the projectile. We are therefore able to measure soft electron spectra correlated to any of these quantities.